

Unraveling Magnetic Anisotropy Energy in Ferromagnetic Monolayer on Ferroelectric ABO₃ via DFT and Machine Learning

Dameul Jeong,¹ Seoung-Hun Kang,^{2,*} and Young-Kyun Kwon^{1,3,†}

¹*Department of Physics, Kyung Hee University, Seoul, 02447, Korea*

²*Materials Science and Technology Division, Oak Ridge National Laboratory, Oak Ridge, TN 37831, United States of America*

³*Department of Information Display and Research Institute for Basic Sciences, Kyung Hee University, Seoul, 02447, Korea*

(Dated: May 2022)

Spin-based devices have attracted attention as an alternative to CMOS-based technology. However, one of the challenges in spintronics devices is reducing the spin-switching energy in ferromagnetic (FM) materials. To address this, we considered ferroelectric (FE) materials, which may affect the magnetic properties of FM materials. We explored various oxide perovskites ABO₃ as FE materials, onto which a Fe monolayer was placed as the FM material. We evaluated the magnetic anisotropy energy (MAE) of the Fe monolayer while varying the polarization of ABO₃. Our analysis showed that the MAE depends on the magnetic dipole moment induced in the FE material at the interface between the FE and FM materials due to structural modifications. Machine learning techniques were also employed to identify universal behaviors of the MAE in the presence of FE layers, confirming the importance of magnetic moments near the interface in explaining the dependence of the MAE on FE materials.

The development of complementary metal-oxide-semiconductors (CMOS) has been driven by the need for small and fast electronic devices. While CMOS has been very successful, its development has stagnated at sizes of 5 nm or less due to the quantum tunneling effect that impedes the smooth movement of electrons in the circuit¹. Despite intensive efforts to overcome this obstacle, finding a fundamental solution remains a challenge²⁻⁴. To resolve such limitations of CMOS, spintronics is emerging as an alternative⁵⁻⁷. Spintronics, which uses the spin of electrons to control devices, has enabled the commercialization of spin-transfer torque (STT) magnetoresistive random access memory (MRAM) with near-zero standby and zero leakage power^{8,9}. However, the energy required to record and maintain magnetic information in STT-MRAM is higher than that of conventional dynamic random access memory (DRAM) as well as static random access memory (SRAM)¹⁰. Therefore, research is being actively conducted to find ways to reduce such high energy consumption¹¹⁻¹³.

Intel developed a spin-based logic device known as magnetoelectric spin-orbit (MESO) several years ago, which outperforms traditional CMOS devices by a factor of 10 to 30. MESO utilizes two physical principles: spin-to-charge conversion through topological and robust spin-orbit coupling (SOC) materials and magnetization switching using the magnetoelectric effect of multiferroic materials such as La-doped BiFeO₃¹⁴. Despite its potential benefits, BiFeO₃ has not been widely used in practical applications due to reliability issues and high costs¹⁵. Furthermore, there are only a few reports of multiferroic materials that exhibit both strong ferromagnetism and ferroelectricity at room temperature, which limits their commercial viability¹⁶. Therefore, new materials and magnetic switching approaches are necessary to develop novel spintronic devices. One possible strategy is

to manipulate the magnetic anisotropy energy (MAE) of ferromagnetic (FM) materials. This involves lowering the energy required to flip a spin, which reduces the write energy requirement. Certain ferroelectric (FE) materials, such as BaTiO₃ and HfO₂, have been shown to modulate the MAE of FM materials through their spontaneous polarization¹⁷⁻²¹.

Here, we report our first-principles and machine learning investigation on the MAE of Fe monolayers in various FE ABO₃ materials, comprising alkaline (A=Ca, Sr, or Ba) and group 4 transition metal (B=Ti, Zr, or Hf) elements. Our study disclosed unusual factors affecting the MAE of Fe monolayers leading to valuable insights that can aid in identifying and improving suitable FE and FM materials for spintronics applications. Specifically, we found that the MAE of Fe monolayers depend not only on the spontaneous polarization of ABO₃ but also on the magnetic dipole moment induced in the FE material near the interface between FE and FM materials due to the structural strain and the proximity effect. Furthermore, we employed a machine learning approach to examine the universal behavior of FM MAE in the presence of FE layers, and our findings demonstrate that the induced magnetic moment near the interface is indeed a crucial feature that can explain the FE-dependent behavior of FM MAE.

We carried out *ab initio* calculations based on density functional theory (DFT)^{22,23} as implemented in the Vienna *ab initio* simulation package (VASP)^{24,25} with projector augmented wave potentials²⁶. For the exchange-correlation (XC) functional, we employed the Ceperley-Alder (CA) form²⁷ within the local density approximation (LDA). The energy cutoff was set to 500 eV for all our calculations. Structural configurations relaxed until the Hellmann-Feynman force on every atom was lower than 0.01 eV/Å. The Brillouin zone was sampled using a 10 × 10 × 10 and a 12 × 12 × 1 Γ -centered k -grids for the

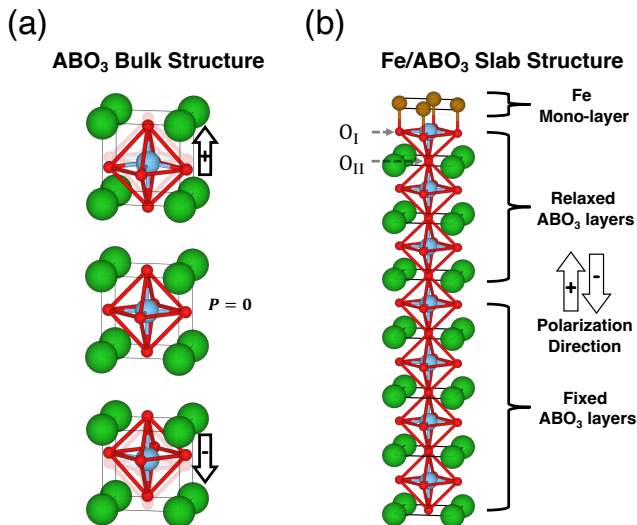


FIG. 1. The Atomic structures of ABO_3 and Fe on ABO_3 with polarization. (a) Three ABO_3 bulk perovskite structures show different polarization states. The Equilibrium structure of bulk ABO_3 is tetragonal in which spontaneous polarization is induced, shown in the top and bottom configurations with the opposite polarization directions, whereas the center one is the central symmetric structure without the spontaneous polarization. (b) Slab model of the Fe monolayer on seven-layer ABO_3 . The lower four layers of the ABO_3 substrate were fixed, and the upper three layers were fully relaxed to describe the bulk and surface effect, respectively. Especially, we named two nonequivalent oxygen atoms near the interface as O_I and O_{II} corresponding to those at the top ABO_3 surface and below the top B atom, respectively.

bulk and slab structures. We considered the spin-orbit interaction and the Berry phase approach²⁸ to evaluate the MAE and the spontaneous polarization, respectively.

To decipher the universal behaviors of the Magnetic Anisotropy Energy (MAE) of the Fe monolayer on ABO_3 , we applied the Sure Independence Screening and Sparsifying Operator (SISSO) approach²⁹. This method prompted us to consider a vast feature space encompassing a wide variety of potential attributes that reflect the essential properties of our Fe monolayer on the ABO_3 slab model. During this process, we put many mathematical operations to work, simple ones such as addition, subtraction, multiplication, and division, and more complex functions like exponentials and trigonometric functions. We put these operations into play between the features, systematically and recursively creating a wealth of meaningful combinations in our system. This thorough, step-by-step approach brought us to six unique features, each with a complexity level of three. We selected a subset of 10,000 features from the abundant collection that we felt deserved a closer look. This in-depth exploration led us to discover an optimized descriptor that beautifully outlines the universal behaviors of the MAE of the Fe monolayer across a variety of ABO_3 compounds.

Perovskite is a mineral with the same crystal form as

$CaTiO_3$, a structure derived from the ABX_3 configuration. Its unit cell is a cube of space group $Pm\bar{3}m$ (221) with cations A and B at the vertices and body centers, respectively, and anion X at the face centers, as illustrated in Figure 1(a). The cation A acts as a fixed shell, so its chemical and physical properties are of relatively little importance, but the displacement of the B and X atoms, which breaks the centrosymmetry transforming the cube into a tetrahedral structure, causes spontaneous polarization. This displacement, which governs the FE properties of perovskites, can be controlled by changing the electronic configuration of the cation B through geometric modification of the BX_6 octahedron³⁰. In this study, only divalent (Group 2: Ca, Sr, Ba, Ra) and tetravalent (Group 4: Ti, Zr, Hf) elements were considered as cations A and B, respectively, and only oxygen as anion X.

To investigate how the FE spontaneous polarization affects the MAE of a Fe monolayer, a slab model was constructed as shown in Figure 1(b). To minimize the lattice mismatch between ABO_3 and the Fe monolayer, we chose the (001) plane of the bcc structure of Fe as the monolayer because it matches very well with the (001) plane of ABO_3 and thus forms a square lattice. We calculated the lattice mismatch between ABO_3 and the Fe monolayer using the Fe bulk lattice constant of 2.75 and obtained the following results: -2.27%, 2.65%, 2.65%, -0.30%, 4.75%, 4.30%, 1.73%, 6.63%, 5.84%, for $CaTiO_3$ (CTO), $CaZrO_3$ (CZO), $CaHfO_3$ (CHO), $SrTiO_3$ (STO), $SrZrO_3$ (SZO), $SrHfO_3$ (SHO), $BaTiO_3$ (BTO), $BaZrO_3$ (BZO), and $BaHfO_3$ (BHO), respectively. We applied a strain only to the Fe monolayer to compensate for these mismatches. The top three layers of the ABO_3 substrate with Fe monolayers were allowed to fully relax to obtain an equilibrium interfacial structure, while the bottom four layers were fixed to maintain the bulk structure that requires spontaneous polarization. The direction of relative displacement of the BO_6 octahedra within the ABO_3 cube determines the direction of polarization, which becomes negative when the octahedron is displaced toward the Fe monolayer, and vice versa.

Having established the interface between the Fe monolayer and ABO_3 substrate, we first studied the MAE of the Fe monolayer on the unpolarized ABO_3 structures with the centrosymmetric structure shown in Figure 1(a). The MAE η is the energy required to change the direction of magnetization from the out-of-plane direction to the in-plane direction in the magnetic thin film material, defined as

$$\eta = E_{\text{tot}}(S_{\rightarrow}) - E_{\text{tot}}(S_{\uparrow}), \quad (1)$$

where $E_{\text{tot}}(S_{\rightarrow})$ and $E_{\text{tot}}(S_{\uparrow})$ are the total energies for the systems with the in-plane (S_{\rightarrow}) and out-of-plane (S_{\uparrow}) spin configurations, respectively. A positive (negative) value of the MAE means that the spin prefers the out-of-plane (in-plane) direction. The MAE arises from the SOC effect, where the orbitals of atoms affected by the crystal field interact with spins³¹. To explore the effects

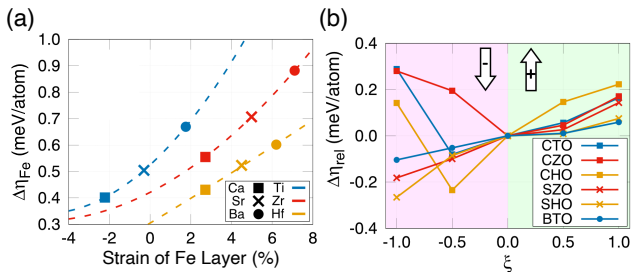


FIG. 2. The relative MAE $\Delta\eta_{\text{Fe}}$, defined in Eq. 2, of the Fe monolayer on various ABO_3 ($A = \text{Ca, Sr, or Ba}$; $B = \text{Ti, Zr, or Hf}$) substrates. Since the lattice mismatch between the Fe monolayer and ABO_3 substrate was released by adjusting the size of the Fe monolayer, the ABO_3 substrate determines the strain of the Fe monolayer. Divalent elements Ca, Sr, and Ba corresponding to the cation A are represented by symbols of solid squares, crosses, and solid circles, whereas tetravalent ones Ti, Zr, and Hf for the cation B are done by colors of blue, red, and yellow, respectively. For each given B atom, $\Delta\eta_{\text{Fe}}$ values for three different A atoms were fitted with a quadratic function, which was plotted with a dashed line with the color corresponding to the B atom. It is clear that the trends of $\Delta\eta_{\text{Fe}}$ are classified by the tetravalent elements. (b) $\Delta\eta_{\text{rel}}$, defined in Eq. 3, as a function of relative polarization ξ of six ABO_3 substrates. The other three ABO_3 substrates are not shown here because their spontaneous polarizations are zero. While $\Delta\eta_{\text{rel}}$ of SZO (red cross), SHO (yellow cross), and BTO (blue circle) show almost linear behaviors, those of CTO (blue square), CZO (red square), and CHO (yellow square) do unexpected upturns as ξ decreases.

of FE substrates alone on the MAE of the Fe monolayer, excluding the strain effect, we evaluated $\Delta\eta_{\text{Fe}}$ defined as

$$\Delta\eta_{\text{Fe}} = \eta_{\text{Fe}/\text{ABO}_3} - \eta_{\text{Fe}_s^{\text{free}}}, \quad (2)$$

where η_X is the MAE of a system X. Here, X is either Fe/ABO_3 or $\text{Fe}_s^{\text{free}}$, which represents a Fe/ABO_3 slab system or a freestanding strained Fe monolayer with the same lattice constant determined by ABO_3 , respectively. As shown in Figure 2(a), the evaluated $\Delta\eta_{\text{Fe}}$ ranges from 0.4 to 0.9 meV/atom on various ABO_3 substrates indicating the out-of-plane spin direction is favored. It is also shown that for a given B element of ABO_3 substrate, the heavier the A element, the higher the MAE. Since the lattice mismatch between the Fe monolayer and ABO_3 substrate was relieved by adjusting the lattice constant of the former as mentioned above, the size of the A atom is directly related to the strain of the Fe monolayer given as the x -axis. The MAE data were well fitted to a quadratic function of the strain of the Fe monolayer for each B element, as shown in Figure 2(a). To explore the inherent effect of the spontaneous polarization of ABO_3 substrate alone on the MAE of the Fe monolayer, we also evaluated the relative MAE $\Delta\eta_{\text{rel}}$ using

$$\Delta\eta_{\text{rel}} = \eta(\xi) - \eta(0), \quad (3)$$

where ξ represents the normalized atomic displacement corresponding to the relative polarization (P) of each

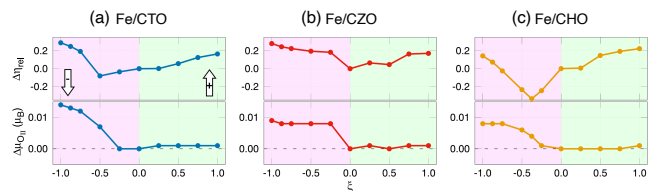


FIG. 3. The relative MAE $\Delta\eta_{\text{rel}}$ and the relative magnetic moments $\Delta\mu_{\text{OII}}$ induced on O_{II} , which is denoted in Figure 1(b), of (a) Fe/CTO, (b) Fe/CZO, and (c) Fe/CHO, as a function of ξ . These relative quantities were evaluated with respect to those of each of the corresponding centrosymmetric systems. The upturns of $\Delta\eta_{\text{rel}}$ as ξ decreases, observed in these cases, are quite strongly correlated with $\Delta\mu_{\text{OII}}$.

ABO_3 with respect to its spontaneous polarization (P_s), or $\xi = P/P_s$. For example, $\eta(0)$ denotes the MAE of the Fe monolayer placed on the corresponding centrosymmetric ($\xi = 0$) ABO_3 substrate with zero polarization. Figure 2(b) presents our evaluated $\Delta\eta_{\text{rel}}$ as a function of ξ . It is noted that negative values in Figure 2(b) do not indicate that the spins on the Fe monolayer prefer the in-plane direction but rather demonstrate the change in MAE with respect to their unpolarized cases, in which the Fe monolayer still favors the out-of-plane spins. In this figure, we did not include three ABO_3 materials, STO, BZO, and BHO, since they are not FE indicating zero spontaneous polarization. Our results demonstrate that the MAE of the Fe monolayer is linearly dependent on ξ on SZO, SHO, and BTO, as naturally expected that the MAE would be affected by the electric field induced by the spontaneous polarization of the substrate. However, when the Fe monolayer is placed on the other three substrates containing Ca element for the A-site, we observed unusual upturns in $\Delta\eta_{\text{rel}}$ as ξ decreases.

We now turn our attention to the abrupt upturns in $\Delta\eta_{\text{rel}}$ observed in three cases (Fe/CTO, Fe/CZO, and Fe/CHO) under the negative spontaneous polarization or $\xi < 0$, as shown in Figure 2(b). It is clear that there must be something other than the induced electric field from spontaneous polarization causing this sudden rise. We found that the MAEs observed in these three cases are governed more strongly by interface effects, such as induced interfacial magnetic dipole moment. As shown in Figure 3, $\Delta\mu_{\text{OII}}$, the relative magnetic moment induced in the oxygen atom O_{II} , located just below the topmost B atom of ABO_3 shown in Figure 1(b), also exhibits a very similar sharp rise. Note that in the other three cases (Fe/SZO, Fe/SZO, and Fe/BTO), where MAE does not show a sharp rise, $\Delta\mu_{\text{OII}}$ remains nearly zero over the entire range of ξ .

Building on these findings, our analysis reveals two distinct factors contributing to the MAE of the Fe monolayer in the ABO_3 systems impacted by spontaneous polarization. The first factor, the "interface effect," is influenced by atomic displacements caused by ferroelectricity. As the spontaneous polarization ξ becomes more

negative, the separation between the Fe and B atoms increases. This displacement subsequently brings the O_{II} atom, as depicted in Figure 1(b), closer to the B atom. The outcome is the induction of a magnetic moment in O_{II}, resulting in an upswing in the MAE following an initial decrease. Simultaneously, the second factor is facilitated by the electric field induced by spontaneous polarization itself. It is particularly prominent in the three cases (Fe/CTO, Fe/CZO, and Fe/CHO), as seen in Figure 3. In these cases, the movement of the B atom, coupled with a reduced magnetic moment at the interface, triggers a magnetic moment in O_{II}, which aligns with the abrupt upturns observed in the MAE of the Fe monolayer (See Supplementary Note S1). Our results underscore the crucial role played by changes in the magnetic moment of interface atoms due to spontaneous polarization. These changes significantly influence the MAE of the Fe monolayer, thus demonstrating the multi-dimensional effects of spontaneous polarization in these complex material systems.

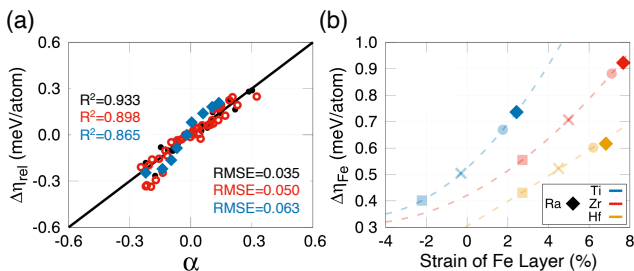


FIG. 4. Machine learning results of the relative MAE $\Delta\eta_{rel}$ for the Fe monolayer on various ABO₃ (A = Ca, Sr, or Ba; B = Ti, Zr, or Hf) substrates and test sets with RaBO₃ (B = Ti, Zr, Hf). (a) Relationship between MAE and descriptors. The descriptor trained for the Fe monolayer on the ABO₃ layer (A = Ca, Sr, Ba; B = Ti, Zr, Hf) were α , while $\Delta\eta_{rel}$ was used for machine learning properties. The solid black circle is a training set with $R^2=0.933$, and the empty red circle is the validation set with $R^2=0.898$. The Blue rhombus point is the test set with $R^2=0.865$. (b) Plotted $\Delta\eta$ of Fe monolayer on the RaBO₃ on top of Figure 2(a). Ra closely follows the trend of the training set.

We employed the Sure Independence Screening and Sparsifying Operator (SISSO) scheme for machine learning to pinpoint the key parameters needed to represent $\Delta\eta_{rel}$ accurately. Training the model on a 30-set that excludes unpolarized ABO₃, we evaluated various features, like atomic bonds of interface atoms, ABO₃'s lattice constant, and individual atom magnetic moments for the Fe monolayer atop the ABO₃ layer (where A = Ca, Sr, Ba; B = Ti, Zr, Hf), in the presence of spontaneous polarization. The ensuing machine-learning model offered the descriptors as follows:

$$\alpha = (\mu_B + \mu_{Fe})(\lambda_1\mu_{O_{II}}\mu_{Fe} + \lambda_2a^6) + \gamma \quad (4)$$

In this equation, α signifies the descriptor, $\lambda_{1,2}$ represent coefficients (with respective values of 1.814×10^3

and 4.312×10^{-4}), and γ is a constant (1.951×10^{-2}). The lattice constant is denoted by a , while μ_B , μ_{Fe} , and $\mu_{O_{II}}$ symbolize the magnetic moments of the B site, Fe, and O_{II} atoms, respectively. Our two-dimensional descriptor α to express $\Delta\eta_{rel}$, not solely based on the magnetic moments of Fe and B atoms, but also integrating the magnetic moment of O_{II} and the lattice constant. Figure 4(a) shows that our descriptor α displays high accuracy ($R^2=0.933$; RMSE=0.035) in predicting $\Delta\eta_{rel}$ for the training set of Fe monolayers on the ABO₃ layer, indicated by solid black circles. Remarkably, our descriptor exhibits accurate prediction values for untrained data ($R^2=0.898$; RMSE=0.050), represented by empty red circles. Furthermore, it performs well for additional ABO₃ types, like RaTiO₃ (not part of the training set) with an R^2 value of 0.865 and RMSE=0.063, denoted by blue rhombi. As shown in Figure 4(b), RaBO₃ (B = Ti, Zr, Hf) closely adheres to the trend of the training dataset demonstrated in Figure 2(b). However, for MgBO₃ (B = Ti, Zr, Hf), the descriptor's prediction of $\Delta\eta_{rel}$ is less accurate, primarily attributed to the A site element's lower atomic weight compared to other ABO₃ compounds. Refer to Supplementary Note S2 for comprehensive details. Thus, our machine learning findings are beneficial for predicting MAE values for Fe monolayers on diverse ABO₃ compounds.

In summary, our study aims to control magnetic anisotropy energy (MAE) in ferromagnetic (FM) materials for low-power spin-based devices by exploring the use of ferroelectric (FE) spontaneous polarization. By examining ABO₃ materials, which can transform into FE, we observed variations in the MAE of a Fe monolayer based on the A and B elements of ABO₃. We discovered a decreasing trend followed by a jump in the MAE due to the interface effect between the Fe monolayer and ABO₃, which was unexpected. Using machine learning, we identified descriptors for physical quantities impacting the MAE and determined that the magnetic moments of interface atoms were the most efficient features. Our machine-learning model demonstrated high accuracy, with an R-square of 0.933 and a root-mean-square error of 0.035. We validated the model by testing it with Ra as one of the A elements and comparing the results to a graph constructed from training elements. Our study highlights how selecting A and B elements in the perovskite structure can affect the magnetic anisotropy energy (MAE) of ferromagnetic (FM) materials, with certain B elements having a more significant impact. It also reveals that the jump in MAE results from the interface effect between the Fe monolayer and ABO₃ rather than the electric field effect due to ABO₃ polarization. The machine learning model developed in this research can help identify the most compelling features for controlling the MAE, such as the magnetic moments of interface atoms. Overall, these findings could enhance the development of efficient spin-based devices and have broad potential applications in materials science.

ACKNOWLEDGMENTS

This research was supported by the Korea government (MSIT) through the National Research Foundation of Korea (NRF-2022R1A2C1005505 and NRF-

2022M3F3A2A01073562) and Institute for Information & Communications Technology Planning & Evaluation (IITP) (2021-0-01580). This work used the resources of the KISTI Supercomputing Center (KSC-2022-CRE-0062 and KSC-2022-CRE-0379).

-
- * Corresponding author. email: physicsksh@gmail.com
 † Corresponding author. email: ykkwon@khu.ac.kr
- ¹ L. Wang, *Quantum mechanical effects on MOSFET scaling limit* (Georgia Institute of Technology, 2006).
 - ² R. Ratnesh, A. Goel, G. Kaushik, H. Garg, Chandan, M. Singh, and B. Prasad, *Materials Science in Semiconductor Processing* **134**, 106002 (2021), ISSN 1369-8001.
 - ³ A. Samal, S. L. Tripathi, and S. K. Mohapatra, *Transactions on Electrical and Electronic Materials* **21**, 443 (2020), ISSN 2092-7592.
 - ⁴ C. Prasad, *IEEE Transactions on Electron Devices* **66**, 4546 (2019).
 - ⁵ S. A. Wolf, D. D. Awschalom, R. A. Buhrman, J. M. Daughton, S. von Molnár, M. L. Roukes, A. Y. Chtchelkanova, and D. M. Treger, *Science* **294**, 1488 (2001).
 - ⁶ I. Žutić, J. Fabian, and S. Das Sarma, *Reviews of Modern Physics* **76**, 323 (2004).
 - ⁷ A. Fert, *Reviews of Modern Physics* **80**, 1517 (2008).
 - ⁸ S. A. Wolf, J. Lu, M. R. Stan, E. Chen, and D. M. Treger, *Proceedings of the IEEE* **98**, 2155 (2010).
 - ⁹ S. Salehi, D. Fan, and R. F. Demara, *ACM Journal on Emerging Technologies in Computing Systems* **13** (2017), ISSN 1550-4832.
 - ¹⁰ T. Nozaki, T. Yamamoto, S. Miwa, M. Tsujikawa, M. Shirai, S. Yuasa, and Y. Suzuki, *Micromachines* **10** (2019), ISSN 2072-666X.
 - ¹¹ Y. Gupta and L. Bhargava, *International Journal of Electronics Letters* **7**, 249 (2019).
 - ¹² V. S. D. Eswar, K. D. Bhavani, and D. Nandan, *Journal of Physics: Conference Series* **1714**, 012041 (2021).
 - ¹³ H. Cai, J. Chen, Y. Zhou, and W. Zhao, *IEEE Transactions on Circuits and Systems II: Express Briefs* **68**, 2633 (2021).
 - ¹⁴ S. Manipatruni, D. E. Nikonov, C.-C. Lin, T. A. Gosavi, H. Liu, B. Prasad, Y.-L. Huang, E. Bonturim, R. Ramesh, and I. A. Young, *Nature* **565**, 35 (2019), ISSN 1476-4687.
 - ¹⁵ J.-C. Yang, Q. He, P. Yu, and Y.-H. Chu, *Annual Review of Materials Research* **45**, 249 (2015).
 - ¹⁶ J. A. Mundy, C. M. Brooks, M. E. Holtz, J. A. Moyer, H. Das, A. F. Rébola, J. T. Heron, J. D. Clarkson, S. M. Disseler, Z. Liu, et al., *Nature* **537**, 523 (2016), ISSN 1476-4687.
 - ¹⁷ C.-G. Duan, S. S. Jaswal, and E. Y. Tsymbal, *Physical Review Letters* **97**, 047201 (2006).
 - ¹⁸ C.-G. Duan, J. P. Velev, R. F. Sabirianov, W. N. Mei, S. S. Jaswal, and E. Y. Tsymbal, *Applied Physics Letters* **92** (2008), ISSN 0003-6951.
 - ¹⁹ P. V. Lukashev, J. D. Burton, S. S. Jaswal, and E. Y. Tsymbal, *Journal of Physics: Condensed Matter* **24**, 226003 (2012).
 - ²⁰ G. Radaelli, D. Petti, E. Plekhanov, I. Fina, P. Torelli, B. R. Salles, M. Cantoni, C. Rinaldi, D. Gutiérrez, G. Panaccione, et al., *Nature Communications* **5**, 3404 (2014), ISSN 2041-1723.
 - ²¹ B. F. Vermeulen, F. Ciubotaru, M. I. Popovici, J. Swerts, S. Couet, I. P. Radu, A. Stancu, K. Temst, G. Groeseneken, C. Adelman, et al., *ACS Applied Materials & Interfaces* **11**, 34385 (2019).
 - ²² P. Hohenberg and W. Kohn, *Physical Review* **136**, B864 (1964).
 - ²³ W. Kohn and L. J. Sham, *Physical Review* **140**, A1133 (1965).
 - ²⁴ G. Kresse and J. Hafner, *Physical Review B* **47**, 558 (1993).
 - ²⁵ G. Kresse and J. Furthmüller, *Physical Review B* **54**, 11169 (1996).
 - ²⁶ P. E. Blöchl, *Physical Review B* **50**, 17953 (1994).
 - ²⁷ D. M. Ceperley and B. J. Alder, *Physical Review Letters* **45**, 566 (1980).
 - ²⁸ N. A. Spaldin, *Journal of Solid State Chemistry* **195**, 2 (2012), ISSN 0022-4596, *polar Inorganic Materials: Design Strategies and Functional Properties*.
 - ²⁹ R. Ouyang, S. Curtarolo, E. Ahmetcik, M. Scheffler, and L. M. Ghiringhelli, *Physical Review Materials* **2**, 083802 (2018).
 - ³⁰ R. J. Tilley, *Perovskites: structure-property relationships* (John Wiley & Sons, 2016).
 - ³¹ G. H. O. Daalderop, P. J. Kelly, and M. F. H. Schuurmans, *Physical Review B* **41**, 11919 (1990).